Geochemistry Geophysics Geosystems G3
AN ELECTRONIC JOURNAL OF THE EARTH SCIENCES
Published by AGU and the Geochemical Society

Technical Brief
Volume 5, Number 12
31 December 2004
Q12D12, doi:10.1029/2004GC000822
ISSN: 1525-2027

Trace element cartography of *Globigerinoides ruber* shells using particle-induced X-ray emission

M. Gehlen
Laboratoire des Sciences du Climat et de l'Environnement, Bât. 709, Orme des Merisiers, CEA/Saclay, F-91191 Gif-sur-Yvette cedex, France (gehlen@cea.fr)

F. Bassinot
Laboratoire des Sciences du Climat et de l'Environnement, Bât. 12, avenue de la Terrasse, F-91198 Gif-sur-Yvette cedex, France

L. Beck
Laboratoire d'Etude des Matériaux par Faisceau d'Ions, L'Institut national des sciences et techniques nucléaires, Département de Recherche sur l'État Condensé, les Atomes et les Molécules, CEA/Saclay, F-91191 Gif-sur-Yvette cedex, France

H. Khodja
Laboratoire Pierre Süe, Bât. 637, CEA/Saclay, F-91191 Gif-sur-Yvette cedex, France

[1] Micro particle-induced X-ray emission (PIXE) is a nondestructive elemental analysis technique that can be used to map the distribution of elements with a spatial resolution of $\pm 4\ \mu m^2$ and a penetration depth of $\pm 2\ \mu m$ in a calcite matrix. To test its potential to improve our understanding of trace element distribution in foraminifera shells, we mapped the Mg distribution across individual chambers of the planktonic species *Globigerinoides ruber*. *G. ruber* shells were picked from equatorial Atlantic surface sediments (Sierra Leone Rise). They ranged from well-preserved to heavily dissolved tests. The mapping of trace elements across test chambers made it possible to discriminate between variability inherent to the shell material and heterogeneity linked to contaminant phases. Contaminating mineral phases were characterized by high Mg concentrations (Mg/Ca = 19.7 mmol/mol) and high levels of Si, Al, and Fe. Mg/Ca values of well-preserved shells ranged from 3.9 to 4.5 mmol/mol. The Mg to Ca ratios of partially dissolved shells varied between 1.8 and 3.4 mmol/mol between outer and inner chambers. Low and homogeneous Mg/Ca values of 2.0 and 2.3 mmol/mol were determined for chambers of a severely dissolved test.

Components: 4516 words, 3 figures, 2 tables.

Keywords: foraminifera; Mg/Ca; dissolution.

Index Terms: 4875 Oceanography: Biological and Chemical: Trace elements; 4894 Oceanography: Biological and Chemical: Instruments and techniques.

Received 24 August 2004; **Revised** 2 November 2004; **Accepted** 19 November 2004; **Published** 31 December 2004.

Gehlen, M., F. Bassinot, L. Beck, and H. Khodja (2004), Trace element cartography of *Globigerinoides ruber* shells using particle-induced X-ray emission, *Geochem. Geophys. Geosyst.*, *5*, Q12D12, doi:10.1029/2004GC000822.

Theme: Biogenic Calcium Carbonate **Guest Editor:** Peggy Delaney

1. Introduction

[2] The Mg to Ca ratio of foraminifer calcite primarily reflects calcification temperature [*Nürnberg et al.*, 1996, 2000; *Lea et al.*, 1999, 2000]. Several studies have proposed to use foraminifera Mg/Ca as a paleotemperature proxy [*Rosenthal et al.*, 1997; *Hastings et al.*, 1998; *Elderfield and Ganssen*, 2000]. The identification and understanding of processes controlling Mg incorporation and distribution in foraminifera shells, as well as of dissolution effects on the primary Mg/Ca signal, is an important issue in foraminiferal trace element research [*Lea*, 1999].

[3] Calcification in bilamellar (perforate) foraminifera results in a layered structure of test walls with a thin, microgranular inner layer covered with a thicker, subrhombic layer [*Bé et al.*, 1975]. Although a few studies provided evidence for a heterogeneous distribution of Mg across bilamellar foraminifera [*Brown and Elderfield*, 1996; *Benway et al.*, 2003; *Eggins et al.*, 2003; *Erez*, 2003], a full understanding of this heterogeneity is still lacking. The study of thick-walled, bilamellar benthic foraminifera suggests that the microgranular layer is precipitated at a higher rate and is enriched in Mg [*Erez*, 2003]. It is not clear yet whether this difference in Mg content between microgranular and subrhombic layers systematically exists in the thinner, planktonic foraminifer shells.

[4] At the end of their life cycle, most planktonic foraminifera secrete a third layer of calcite made of randomly oriented euhedral crystals, which covers the primary (ontogenic) calcite layers. The importance of this third layer (secondary or gametogenic calcite) is species-dependent. Gametogenesis of deep-dwelling, planktonic foraminifera usually takes place in cold deep waters which would imply the deposition of a low Mg calcite. However, in the case of foraminifera cultured under constant temperature conditions, *Nürnberg et al.* [1996] found significantly higher Mg concentrations in tests after specimens released gametes. It is likely that gametogenetic calcite of planktonic foraminifera found in deep-sea sediments carries a complex Mg signal reflecting an environmental temperature imprint superimposed on physiological (kinetic) effects. In addition, the life cycle of some planktonic foraminifer species (e.g., *Neogloboquadrina dutertrei*) involves extensive migration in the water column and thus habitat modification [*Hemleben*, 1989]. Life cycle characteristics are reported to be at the origin of species-dependent heterogeneities in Mg/Ca across shells, the different chambers reflecting the mean temperature and chemistry of water masses where chamber calcification took place [*Eggins et al.*, 2003].

[5] Finally, the primary signal carried by the Mg concentration of foraminifer calcite could be altered during seafloor dissolution, which preferentially removes Mg enriched fractions [e.g., *Brown and Elderfield*, 1996; *Benway et al.*, 2003]. The preferential dissolution is evidenced by the decrease of Mg/Ca ratios with increasing water depth of deposition in the ocean [*Brown and Elderfield*, 1996; *Rosenthal et al.*, 2000; *Dekens et al.*, 2002; *Beck et al.*, 2002]. Laboratory dissolution experiments and field observations [e.g., *Bé et al.*, 1975; *Bonneau et al.*, 1980; *Benway et al.*, 2003] document the preferential removal of the inner microgranular layer during early stages of dissolution. On the contrary, the gametogenic or secondary calcite is known for its greater resistance [*Benway et al.*, 2003, and references therein]. These differences in dissolution susceptibility are poorly understood, although the Mg concentration and/or perfection of calcite lattice (crystallinity [*Bassinot et al.*, 2004]) probably play a major role.

[6] Many unknowns regarding the Mg signal in foraminifer calcite remain. Our understanding of processes which control the incorporation of Mg (kinetic versus thermodynamic) and of mechanisms involved in its loss during dissolution will benefit from a method allowing the mapping of Mg distributions across individual shells. Only a limited number of studies have addressed the heterogeneity of Mg/Ca in foraminifera shells, either along discrete profiles (1-D) across the shell walls [*Brown and Elderfield*, 1996; *Eggins et al.*, 2003; *Erez*, 2003] or, indirectly, though the progressive dissolution of foraminifera shells [*Benway et al.*, 2003]. In order to get a step further, there is a need to map (2-D) the Mg distribution across foraminifera shells. In this study, we address the potential of particle-induced X-Ray emission (PIXE), a nondestructive elemental analysis technique, to complement existing wet chemical and physical methods by mapping the Mg distribution across individual chambers of foraminifera shells. We selected *Globigerinoides ruber*, a surface dwelling species known to calcify over a narrow depth range [*Hemleben*, 1989] and commonly used for ocean temperature reconstructions. The PIXE imaging

(with a pixel resolution of ±4 μm^2) is used to evaluate the effects of dissolution on the distribution of Mg across the shells.

2. Material

[7] Foraminifera were picked from core top sediments collected in the Equatorial Atlantic (Sierra Leone Rise) at water depths of 2637 m (station A: 5°07 N, 21°01 W, bottom water CO_3^{2-} = 113.4 μmol/kg, Ω_c = 1.60), 3147 m (station B: 5°25 N, 21°31 W, bottom water CO_3^{2-} = 112.9 μmol/kg, Ω_c = 1.44) and 4202 m (station E: 7°00 N, 24°37 W, bottom water CO_3^{2-} = 110.2 μmol/kg, Ω_c = 1.15). The saturation index with respect to calcite, Ω_c, is defined as the ratio between the in situ concentration product $[Ca^{2+}] \times [CO_3^{2-}]$ over the stoichiometric calcite solubility product after *Mucci* [1983]. Sediments were retrieved with a multicorer. Sediments were extruded and core tops were sliced to get 1 cm thick samples. Sediment samples were transferred into plastic containers and stored at 2°C without further conditioning or processing. Core top sediments were subsampled on shore. Sediments were gently sieved over a 150 μm sized mesh. The coarse fraction was purified by repeated sonification and rinsing with distilled water before being dried over night at 50°C. *G. ruber* shells were handpicked in the 250–315 μm range. Shells were soaked in methanol and ultrasonically cleaned in order to remove fines that could fill the last chambers.

[8] Ten to 30 shells were embedded in epoxy resin and polished with diamond paste. Shells for PIXE analysis were selected under a light microscope. Only shells polished along an orthogonal plane across shell walls were retained for this study. The pores crosscutting the shell walls are clearly distinguishable in this case.

3. Methods

[9] We selected particle-induced X-ray emission (PIXE) for the multielemental analysis (Na to Fe) and cartography of foraminifer shell samples. PIXE is a nondestructive elemental analysis technique [*Johansson and Campbell*, 1988; *Johansson et al.*, 1995; *Moretto and Beck*, 2003, 2004]. The interaction between charged particles with an energy of several MeV and the atoms of the sample matrix leads to the ionization of inner atomic shell electrons. The filling of the resulting inner shell vacancies by electron transitions from outer shells leads to the emission of element characteristic X rays (and Auger electrons).

[10] As a standard procedure, PIXE analyses are run using protons as incident particles. For this study, we selected helium ions instead of protons [*Beck et al.*, 2002]. The use of helium ions has two advantages: (1) the reduction of the spectrum background and (2) the reduction of the penetration depth and thus of the volume analyzed (L. Beck, Improvement in detection limits by using helium ion as particle induced X-ray emission, submitted to *X-ray Spectrometry*, 2004). Both combine to reduce the detection limit of Mg in calcite. The validity of helium induced PIXE for the determination of low Mg concentrations in a calcite matrix was the focus of an earlier study [*Beck et al.*, 2002]. *Beck et al.* [2002] report a detection limit of 50 ppm for Mg in a calcite matrix. They further compare results obtained by PIXE and ICP-AES. The overall agreement between both methods was satisfying.

[11] Experiments were carried out at the nuclear microprobe (micro-PIXE) of the Pierre Suë Laboratory [*Khodja et al.*, 2001] with a 2 MeV helium ion beam set to a 2 μm by 2 μm cross section. The penetration depth of a 2 MeV helium ion beam in calcite is ≈6 μm. X rays are attenuated by the sample matrix and the majority (95%) of the detected X rays originates from the 2 to 2.5 upper micrometers. Hence the analyzed volume corresponds to ≈8 μm^3. While the spatial resolution allows for the analysis of individual chambers of *G. ruber* tests, the heterogeneity at the level of the individual calcite layer (e.g., microgranular, respectively subrhombic) is not resolved.

[12] X rays were collected with a 50 mm^2 Si (Li) detector. For each shell chamber, 1 to 3 images were recorded. Depending on its size, data acquisition took between 2 and 4 hours per image. Images were processed with RISMIN [*Daudin et al.*, 2003]. This software enables the acquisition of X-ray spectra and the 2-D mapping of element distributions based on the number of X rays emitted by the element of interest. While the surface resolution depends solely on the spot size and is element independent, the penetration depth varies slightly between elements as a function of the energy of emitted X rays. For example, the Mg-K line at 1.25 keV is more attenuated by the

matrix than the Ca-K_α line at 3.69 keV. The Mg cartography represents the X-ray counts integrated over ±2 μm depth, while the Ca cartography those integrated over a depth of ±2.5 μm. Because of the difference in penetration depths, the mapping of Mg to Ca ratios at the pixel scale is not appropriate. Thus each image presented in this paper shows the distribution of the X-ray emissions of a single element across the foraminifer shell.

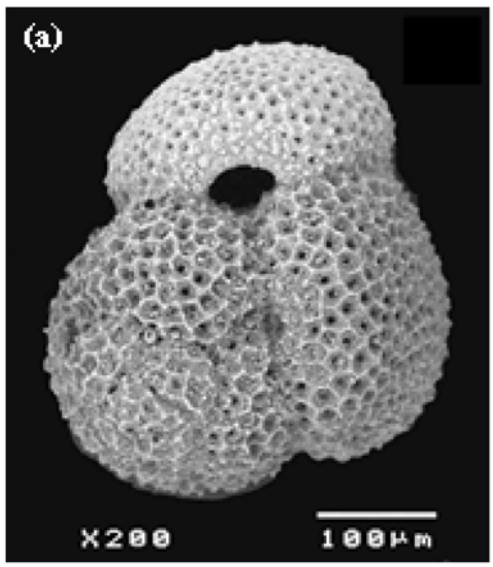

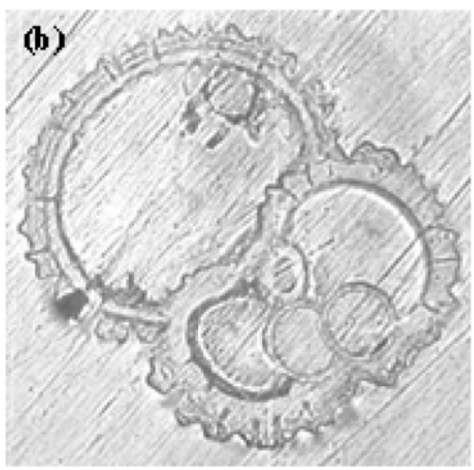

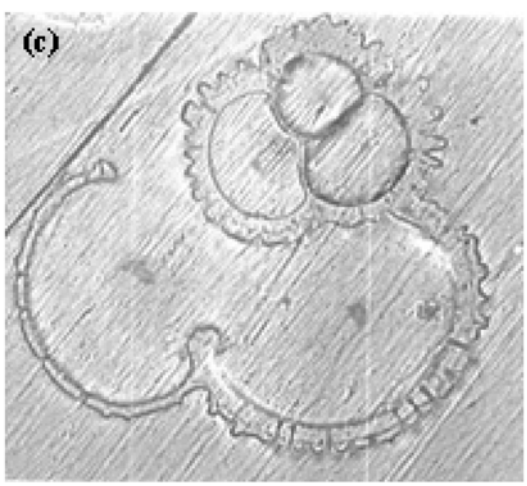

[13] Elemental concentrations were calculated using GUPIX [*Maxwell et al.*, 1989; *Hopman et al.*, 2002] after selecting representative areas on each image produced by RISMIN. Selected areas have to be as homogenous as possible and far from the edge of the shell in order to avoid the transition between the shell and the resin. Elemental concentrations calculated by GUPIX are corrected for differences in penetration depth.

4. Results

[14] Examples of shells of *G. ruber* picked from surface sediments recovered from 3147 m water depth on Sierra Leone Rise are presented on Figure 1. The SEM picture (Figure 1a) shows an ultrasonically cleaned shell of *G. ruber* prior to embedding in epoxy resin. The shell appears to be well preserved and free of adhering clay particles. On Figure 1b a cross section of a well-preserved *G. ruber* shell included in epoxy resin and polished is presented. The layered structure of the shell wall with successive microgranular and subrhombic calcite layers can be distinguished on the section across the upper chamber. A section across a *G. ruber* shell with signs of corrosion (thinner chamber walls) is shown on Figure 1c.

4.1. Trace Element Cartography

[15] Maps of trace element distribution across the area surrounding early chambers (in the sense of the first chambers formed by the organism) of a well-preserved foraminifer shell separated from core top sediments of station A (2637 m) are shown in Figure 2. The chamber

Figure 1. (a) Scanning electronic microscope (SEM) picture of a well-preserved *Globigerinoides ruber* shell picked from surface sediments recovered from 3147 m water depth on Sierra Leone Rise. (b) Cross section of a well-preserved *G. ruber* shell included in epoxy resin and polished. Size of picture is 300 μm. Note the layered structure of the shell wall and the presence of crosscutting pores. (c) Example of a section across *G. ruber* shell with signs of dissolution. Note thinning of final chamber. Size of picture is 350 μm.

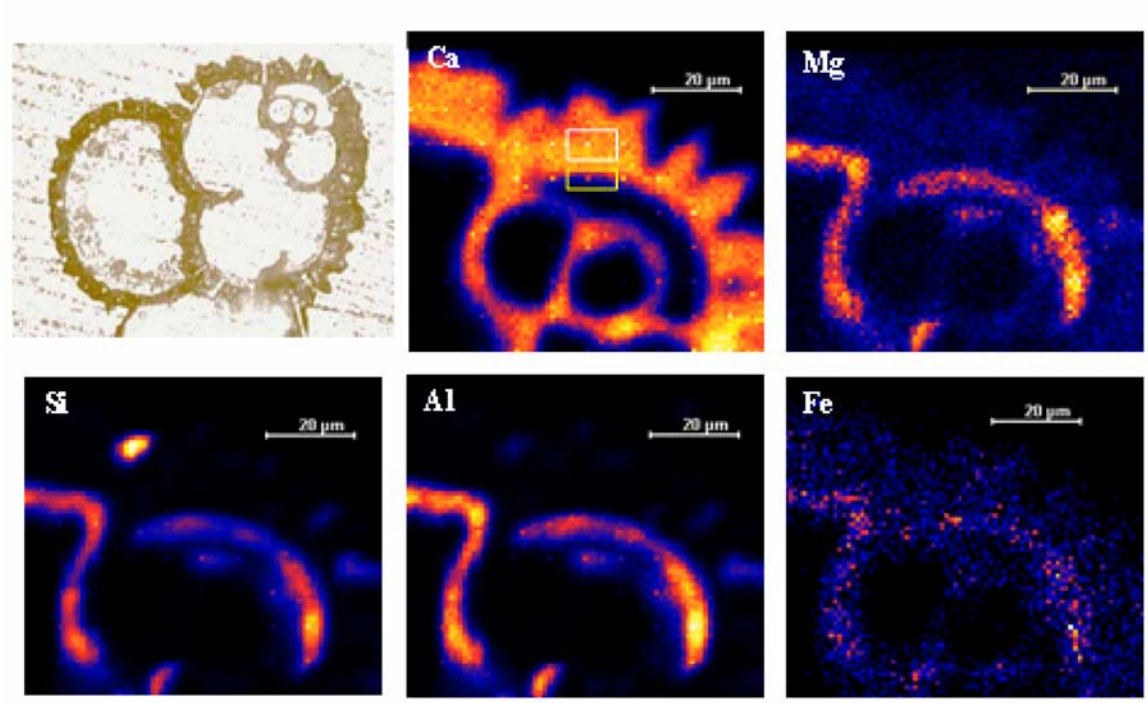

Figure 2. Example of element mapping. Areas analyzed are as follows: bulk shell material, white rectangle; coating, yellow rectangle. X-ray counts are represented for each element on an arbitrary color scale (brightness increases with X-ray counts).

inner walls are enriched in Mg, but also in Si, Al and Fe. A close examination of Figure 2 reveals that the zones enriched in trace elements are adhering to the chamber walls. We analyzed the composition of the bulk carbonate material and of the chamber coating (Table 1). A Mg to Ca ratio of 19.7 mmol/mol was determined for the coating, compared to 3.9 mmol/mol for the bulk chamber calcite. The high levels of Mg are associated with high levels of trace elements quantified by PIXE (Table 1). Only Mg/Ca ratios obtained for the bulk chamber calcite are presented hereafter.

4.2. Mg to Ca Ratios Across *G. ruber* Shells

[16] In order to assess the variability of Mg/Ca ratios across *G. ruber* shells, we identified three regions for PIXE analysis: early (I), intermediate (II) and final (III) chambers (Figure 3). The spatial distribution of Ca and Mg is shown for each of the three regions. In order to estimate the variability of Mg/Ca within a given shell region, we analyzed the elemental composition of 3 to 5 areas within the selected region of samples B2, E1 and E2. Mean values and standard deviations are summarized in Table 2. The standard deviation ranges between 6 and 14 % of the mean. It reflects the reproducibility of the method (±5%) and the variability of the biogenic material.

[17] The Mg to Ca ratio of shell region I of a foraminifer test picked from core top sediments from 2637 m water depth was 3.9 mmol/mol. The Mg/Ca ratios measured for shells originating from 3147 m water depths varied from 3.9 to 4.9 mmol/mol between individual shells (B1, B2, B3) and shell regions (I, II, III). The average Mg/Ca ratio for shell B1 computed by combining

Table 1. Trace Element Composition of Chamber Wall and Adhering Coating

	Trace Element Normalized to Ca, mmol/mol	
Trace Element	Chamber Wall	Coating
Na	3.4	7.1
Mg	3.9	19.7
Al	1.3	140.2
Si	3.3	270.5
P	0.0	6.3
S	4.6	13.2
Cl	3.6	13.2
K	3.1	23.2
Fe	0.0	59.5
Ti	0.0	4.4

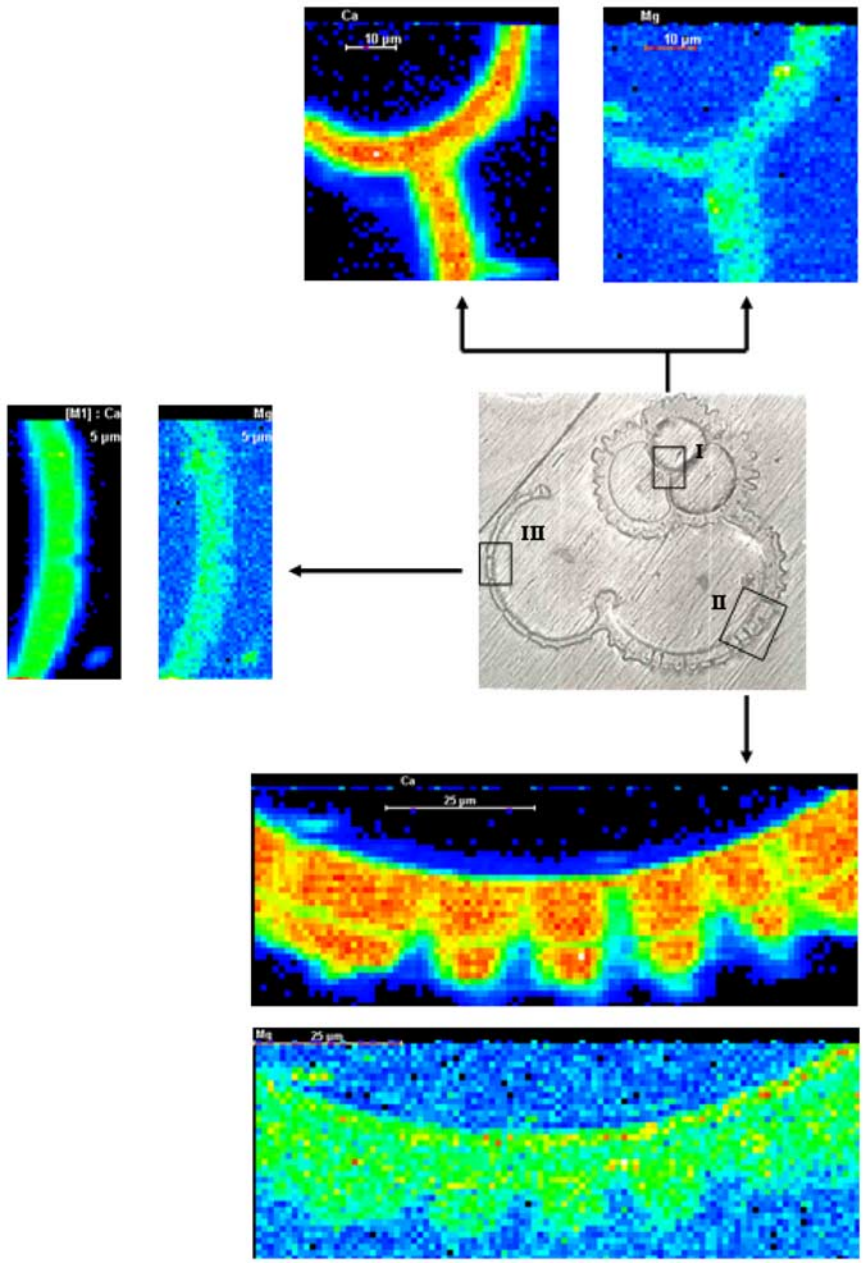

Figure 3. Regions identified for PIXE analysis on a single foraminifera shell (in this case the shell shown on Figure 1c). A distinction is made between early (I), intermediate (II) and final (III) chambers. The spatial distribution of Ca and Mg is shown for each of the three regions. X-ray counts are represented for each element on an arbitrary color scale (brightness increases with X-ray counts).

measurements from different shell regions was 4.4 ± 0.4 mmol/mol. The corresponding average of B3 was 4.0 ± 0.1 mmol/mol. The standard deviation of the mean value computed for different shell regions is smaller, respectively comparable to the one associated with repeated measurements over the same shell region (B2). Thus the variability of Mg/Ca across the shell is of the same order of magnitude as the variability at the level of the individual chamber. It follows that Mg is homogeneously distributed across shells B1, B2 and B3 at the level of the resolution of our method.

[18] The Mg to Ca ratio of shells picked in sediments from 4202 m depth varies between 1.8

Table 2. Elemental Composition of Foraminifer Shell Chambers

Sample	Water Depth, m	Chamber Growth Sequence Mg/Ca, mmol/mol				Shell Aspect/Preservation
		I (Early)	II	II	III (Final)	
A1	2637	3.9				well preserved
B1	3147	4.4	4.9		4.0	thin final chamber
B2	3147	4.0 ± 0.5			4.5 ± 0.3	well preserved
B3	3147	3.9	4.1		3.9	well preserved
E1	4202	3.1	3.4	2.6	1.8 ± 0.2	partially dissolved
E2	4202	2.0	2.3		2.3	severely dissolved
E3	4204		3.3 ± 0.3		2.2 ± 0.2	partially dissolved

and 3.4 mmol/mol. They are significantly lower than their shallow water counterparts. A gradient between the early (Mg/Ca = 3.1 mmol/mol) and the final chambers (Mg/Ca = 1.8 mmol/mol) was detected for the partially dissolved sample E1. The variability of Mg/Ca estimates for different shell regions exceeds the within region variability. For sample E1, dissolution has resulted in a pronounced decrease of Mg/Ca of the final chamber. The severely dissolved shell E2 was characterized by low average Mg/Ca values of 2.2 ± 0.2 mmol/mol. They were homogenously distributed across the shell. The overall lower Mg/Ca ratios of partially dissolved shells, is compatible with the preferential loss of $MgCO_3$.

5. Discussion

5.1. Trace Element Cartography

[19] The analysis of the trace element distribution across a shell wall (Figure 2 and Table 1) reveals a zone enriched in trace elements adhering to the inner chamber wall. The high Mg to Ca ratio of 19.7 mmol/mol determined for the coating is associated with overall high levels of trace elements.

[20] The presence of trace element enriched layers on inner and outer chamber walls of shells of several foraminifer species was acknowledged by *Eggins et al.* [2003]. The authors used high-resolution laser ablation ICP-MS with an ablation volume of ±2 μm^3 to study the compositional variability within several foraminifer species including *G. ruber*. The spatial resolution allowed the identification of a 1 to 3 μm thick surface veneer enriched in Mg, Mn, Zn and Ba on the shell surface of live-sampled and fossil *G. ruber* shells. Besides the compositional signature of the surface veneer, the composition of the bulk wall was homogenous. Because of the coarser resolution of micro-PIXE, the presence of a surface veneer could not be verified during this study. In addition to the lack of resolution, the elements Mn, Zn and Ba can not be analyzed by PIXE under experimental conditions optimized for the measurement of low Mg levels.

[21] In the present study, the composition of the zone enriched in trace elements detected by PIXE (Table 1) points toward a contamination by adhering clay particles (Al/Si ≈ 0.5 mol/mol). The presence of contaminating mineral phases, if uncorrected, is at the origin of an overestimation of Mg to Ca ratios determined by bulk chemical methods such as ICP-AES. The potential problems linked to the presence of silicate minerals in foraminifer samples has been acknowledged and appropriate cleaning methods have been proposed [*Barker and Elderfield*, 2001; *Barker et al.*, 2003]. *Barker et al.* [2003] proposed a means for correcting ICP-AES results for the error associated with the mineral contamination which takes into account the Fe/Mg or Al/Mg ratios of the contaminant and the sample. The chemical cleaning might however alter the primary signal of samples. In the case of PIXE the compositional information provided by the analytical technique allows for a direct discrimination between contaminated areas and clean foraminifer shell material.

5.2. Mg to Ca Ratios of *G. ruber* Shells

[22] The analysis of Mg/Ca variability in *G. ruber* sampled at 3147 m water depth indicates an initial homogenous distribution of Mg across the foraminifer test at the level of resolution of our method. A rather homogenous distribution of Mg across inner walls of *G. ruber* shells was also documented by *Eggins et al.* [2003]. It is explained in terms of

the life cycle of this near-surface-dwelling foraminifer species which calcifies over a small depth range [*Hemleben*, 1989].

[23] The significantly lower Mg/Ca of shell samples originating from 4202 m water depth suggests that dissolution is accompanied by the preferential loss of $MgCO_3$. Preferential dissolution might be at the origin of the heterogeneity in Mg distribution seen in the partially dissolved sample E1. For this particular sample, dissolution has resulted in a pronounced decrease of Mg/Ca of the final chamber. Dissolution appears to progress from the final (outer) to the early (inner) chamber. A similar order of dissolution was reported by *Hecht et al.* [1975] for *G. sacculifer* tests. This order does not contradict the observation of the rapid removal of the inner microgranular layer during early stages of dissolution [*Benway et al.*, 2003]. The inner chamber corresponds to a microenvironment characterized by only very limited exchange with the surrounding fluid. Under these conditions products of organic carbon decay are expected to build up rapidly, thereby leading to a saturation of the microenvironment with respect to calcite. Carbonate dissolution will cease. The outer chambers are in contact with pore waters allowing for the diffusive transport of reaction products away from the shells. In addition, shells are mixed across chemical gradients by bioturbation. These factors combine to promote dissolution compared to what happens in microenvironments and might explain the observed heterogeneity of Mg across the shell sample E1.

Acknowledgments

[24] We would like to acknowledge D. Eliot for his time and assistance in sample preparation. The manuscript benefited from the insightful comments by two anonymous reviewers and H. Elderfield (associate editor). This is LSCE contribution 1122.

References

Barker, S., and H. Elderfield (2001), Core-top calibrations of foraminiferal Mg/Ca from a North Atlantic transect: Refining Mg/Ca paleothermometry, *Eos Trans. AGU*, *82*(47), Fall Meet. Suppl., Abstract PP12A-68.

Barker, S., M. Greaves, and H. Elderfield (2003), A study of cleaning procedures used for foraminiferal Mg/Ca paleothermometry, *Geochem. Geophys. Geosyst.*, *4*(9), 8407, doi:10.1029/2003GC000559.

Bassinot, F. C., F. Mélières, M. Gehlen, C. Levi, and L. Labeyrie (2004), Crystallinity of foraminifera shells: A proxy to reconstruct past bottom water $CO_3^=$ changes?, *Geochem. Geophys. Geosyst.*, *5*, Q08D10, doi:10.1029/2003GC000668.

Bé, A. W. H., J. W. Morse, and S. M. Harrison (1975), Progressive dissolution and ultrastructural breakdown in planktonic foraminifera, in *Dissolution of Deep-Sea Carbonates*, edited by W. V. Sliter, A. W. H. Bé, and W. H. Berger, *Spec. Publ. Cushman Found. Foraminiferal Res.*, *13*, 27–55.

Beck, L., F. Bassinot, M. Gehlen, P. Trouslard, S. Pellegrino, and C. Levi (2002), Detection limit improvement for Mg in marine foraminiferal calcite by using helium induced X-ray emission, *Nucl. Instrum. Methods Phys. Res., Sect. B*, *190*, 482–487.

Benway, H. M., B. A. Haley, G. P. Klinkhammer, and A. C. Mix (2003), Adaptation of a flow-through leaching procedure for Mg/Ca paleothermometry, *Geochem. Geophys. Geosyst.*, *4*(2), 8403, doi:10.1029/2002GC000312.

Bonneau, M. C., F. Mélières, and C. Vergnaud-Grazzini (1980), Variations isotopiques (oxygène et carbone) et crystallographiques chez des espèces actuelles de foraminifères planctoniques en fonction de la profondeur de dépôt, *Bull. Soc. Geol. Fr.*, *22*(5), 791–793.

Brown, S., and H. Elderfield (1996), Variations in Mg/Ca and Sr/Ca ratios of planktonic foraminifera caused by postdepositional dissolution: Evidence of shallow Mg-dependent dissolution, *Paleoceanography*, *11*(5), 543–551.

Daudin, L., H. Khodja, and J. P. Gallien (2003), Development of "position-charge-time" tagged spectrometry for ion beam microanalysis, *Nucl. Instrum. Methods Phys. Res., Sect. B*, *210*, 153–158.

Dekens, P. S., D. W. Lea, D. K. Pak, and H. J. Spero (2002), Core top calibration of Mg/Ca in tropical foraminifera: Refining paleotemperature estimation, *Geochem. Geophys. Geosyst.*, *3*(4), 1022, doi:10.1029/2001GC000200.

Eggins, S., P. De Deckker, and J. Marshall (2003), Mg/Ca variation in planktonic foraminifera tests: Implications for reconstructing palaeo-seawater temperature and habitat migration, *Earth Planet. Sci. Lett.*, *212*, 291–306.

Elderfield, H., and G. Ganssen (2000), Past temperature and $\delta^{18}O$ of surface ocean waters inferred from foraminiferal Mg/Ca ratios, *Nature*, *405*, 442–445.

Erez, J. (2003), The source of ions for biomineralization in foraminifera and their implications for paleoceanographic proxies, in *Biomineralization*, *Rev. Mineral. Geochem.*, vol. 54, edited by P. M. Dove, J. J. De Yoreo, and S. Weinder, pp. 115–149, Mineral. Soc. of Am., Washington, D. C.

Hastings, D. W., A. D. Russel, and S. R. Emerson (1998), Foraminiferal magnesium in *Globeriginoides sacculifer* as a paleotemperature proxy, *Paleoceanography*, *13*(2), 161–169.

Hecht, A. D., E. V. Eslinger, and L. B. Garmon (1975), Experimental studies on the dissolution of planktonic foraminifera, in *Dissolution of Benthic Carbonates*, edited by W. V. Sliter, A. W. H. Bé, and W. H. Berger, *Spec. Publ. Cushman Found. Foraminiferal Res.*, *13*, 56–69.

Hemleben, C. (1989), *Modern Planktonic Foraminifera*, Springer, New York.

Hopman, T. L., Z. Nejedly, J. A. Maxwell, and J. L. Campbell (2002), Extension of GUPIX to H-2, He-3 and He-4 excitation, *Nucl. Instrum. Methods Phys. Res., Sect. B*, *189*, 138–142.

Johansson, S. A. E., and J. L. Campbell (1988), *PIXE: A Novel Technique for Elemental Analysis*, John Wiley, Hoboken, N. J.

Johansson, S. A. E., J. L. Campbell, and K. Malmqvist (1995), *Particle-Induced X-ray Emission Spectrometry (PIXE)*, vol. 133, Chemical Analysis, Wiley, New York.

Khodja, H., E. Berthoumieux, L. Daudin, and J. P. Gallien (2001), The Pierre Sue Laboratory nuclear microprobe as a multi-disciplinary analysis tool, *Nucl. Instrum. Methods Phys. Res., Sect. B*, *181*, 83–86.

Lea, D. W. (1999), Trace elements in foraminiferal calcite, in *Modern Foraminifera*, edited by B. K. Sen Gupta, pp. 259–277, Springer, New York.

Lea, D. W., T. A. Mashiotta, and H. J. Spero (1999), Controls of magnesium and strontium uptake in planktonic foraminifera determined by live culturing, *Geochim. Cosmochim. Acta*, *63*(16), 2369–2379.

Lea, D. W., D. K. Pak, and H. J. Spero (2000), Climate impact of late Quaternary equatorial Pacific sea surface temperature variations, *Science*, *289*, 1719–1724.

Maxwell, J. A., J. L. Campbell, and W. J. Teesdale (1989), The Guelph PIXE software Package, *Nucl. Instrum. Methods Phys. Res., Sect. B*, *43*, 218–230.

Moretto, P., and L. Beck (2003), Emission X induite par particules chargées (PIXE): Théorie, *Tech. Ing.*, *2557*, 1–8.

Moretto, P., and L. Beck (2004), Emission X induite par particules chargées (PIXE): Applications, *Tech. Ing.*, *2558*, 1–17.

Mucci, A. (1983), The solubility of calcite and aragonite in seawater at various salinities, temperatures, and one atmosphere total pressure, *Am. J. Sci.*, *283*, 780–799.

Nürnberg, D., J. Bijma, and C. Hemleben (1996), Assessing the reliability of magnesium in foraminiferal calcite as a proxy for water mass temperatures, *Geochim. Cosmochim. Acta*, *60*(5), 803–814.

Nürnberg, D., A. Müller, and R. R. Schneider (2000), Paleo-sea surface temperature calculations in the equatorial east Atlantic from Mg/Ca ratios in planktic foraminifera: A comparison to sea surface temperature estimates from $U^{k'}_{37}$, oxygen isotopes, and foraminiferal transfer function, *Paleoceanography*, *15*(1), 124–134.

Rosenthal, Y., E. A. Boyle, and N. Slowey (1997), Temperature control on the incorporation of magnesium, strontium, fluorine, and cadmium into benthic shells from Little Bahama Bank: Prospects for thermocline paleoceanography, *Geochim. Cosmochim. Acta*, *61*(17), 3633–3643.

Rosenthal, Y., G. P. Lohmann, K. C. Lohmann, and R. M. Sherrell (2000), Incorporation and preservation of Mg in *Globigerinoides sacculifer*: Implications for reconstructing the temperature and $^{18}O/^{16}O$ of seawater, *Paleoceanography*, *15*(1), 135–145.